PAPER

Experimental quantum polarimetry using heralded single photons

View the article online for updates and enhancements.

Experimental quantum polarimetry using heralded single photons

Seung-Jin Yoon[1], Joong-Sung Lee[1], Carsten Rockstuhl[2,3], Changhyoup Lee[2]
and Kwang-Geol Lee[1]

[1] Department of Physics, Hanyang University, Seoul 04763, Republic of Korea
[2] Institute of Theoretical Solid State Physics, Karlsruhe Institute of Technology, 76131 Karlsruhe, Germany
[3] Institute of Nanotechnology, Karlsruhe Institute of Technology, 76021 Karlsruhe, Germany

E-mail: changhyoup.lee@gmail.com and kglee@hanyang.ac.kr

Abstract

We perform experimental quantum polarimetry using a heralded single photon to analyze the optical activity of linearly polarized light traversing a chiral medium. Three kinds of estimators are considered to estimate the concentrations of sucrose solutions from measuring the rotation angle of the linear polarization of the output photons. Through repetition of independent and identical measurements performed for each individual scheme and different concentration sucrose solutions, we compare the estimation uncertainty among the three schemes. The results are also compared to classical benchmarks for which a coherent state of light is taken into account. The quantum enhancement in the estimation uncertainty is evaluated and the impact of experimental and technical imperfections is discussed. In this work, we lay out a route for future applications relying on quantum polarimetry.

Keywords: optical activity, chirality, single photon, heralded single photon, polarimetry, quantum polarimetry, estimation

(Some figures may appear in colour only in the online journal)

1. Introduction

Optical activity causes rotation of the linear polarization of light when it traverses a chiral material, i.e. a material made from entities that lack mirror symmetry. The measurement of such optical activity has often been used in pharmacology, where it is important to study the chirality of drug molecules, which determines their toxicity and efficacy, originating from the relative handedness of the enantiomers [1, 2]. Chirality has also been explored in various other fields, including chemistry, life science, physics, and material science, where polarimetric schemes provide rich information about molecular or nano-photonic chiral structures [3–8].

A variety of detection schemes have been developed for measuring the optical activity, i.e. analyzing the rotation of the linear polarization of light upon propagation through a chiral medium [9–11]. This rotation of the polarization has its origin in the different propagation constants for the two counter-rotating circularly polarized plane waves, which are eigenmodes of the chiral medium and into which the linear polarization can be decomposed. The estimated direction of linear polarization will fluctuate due to the discrete nature of light even when the chirality is fixed and experimental noise is removed. These fluctuations determine the reliability of the measurement, often called the precision, which reflects the data quality. In general, the precision increases with the intensity N (or the average photon number) of the light used. However, there exist situations in which the intensity of the incident light impinging on an analyte is required to be limited, when sample damage or any unwanted side effects occur in the high intensity regime, e.g. when the non-linear dependence is significant. Also, light itself can trigger unwanted chemical reactions in the molecular material to be detected [12–15]. The presence of such constraints has inspired the development of quantum metrological approaches over the last few decades. The aim is to improve the data quality while keeping the incident power in the low intensity regime [16, 17], i.e. improving the precision for a fixed intensity.

Probing analytes with quantum states of light promises detection with much reduced noise, below what is possible with classical states of light, thus allowing better performance in optical measurements [18–20]. In particular, the phase-sensitive N00N states have been adopted to measure the chirality. For example, the Faraday rotation in a rubidium vapor cell has been measured with polarization N00N states, showing that the standard quantum limit can be beaten [21]. The dispersion of optical rotation has also been analyzed by injecting polarization-entangled states with different and tunable wavelengths [22]. Chemical processes that change the chirality of molecules have been monitored in real-time with polarization N00N states with a protocol in the context of quantum phase estimation [23, 24]. In addition to schemes measuring the chirality, N00N states have been employed to achieve a quantum enhancement in other sensing scenarios, such as in the measurement of the refractive index of blood proteins [25], quantum lithography [26], and super-sensitive microscopy [27, 28]. The superior optical detection shown with the N00N states originates from the quantum entanglement of photons, leading to a higher signal-to-noise ratio ($\sqrt{N}$ times larger) when compared to measurements that rely on classical sources such as coherent states of light. The quantum advantage enabled by N00N states is known to be vulnerable to photon loss or decoherence [29, 30], but one can use optimally engineered definite photon-number states that always outperform the standard quantum limit for a given loss [31–33].

In the context of polarimetry, the chirality of a molecular solution is measured by measuring the transmittance T of a linearly polarized incident light passing through an analyte resolved in its co-or cross-polarized components. For definiteness we speak in the following of horizontal and vertical polarization. The presence of the chiral medium rotates the polarization weakly, which can be probed from the change of the intensity of the incidence polarization or from the difference between horizontally and vertically polarized light. From these measured intensities we can determine the concentration of molecules if the chirality itself is known. It is known that the photon number state $|N\rangle$ is the optimal state that minimizes the noise in the transmission measurement [34, 35]. This is because the photon number state has no uncertainty in its intensity, offering the most precise detection when monitoring a change of the intensity [36, 37]. Unlike N00N states, the photon number state always offers a quantum gain in noise reduction at any loss level $\gamma \ (= 1 - \eta)$, exhibiting a detection fluctuation $\Delta_q T = \sqrt{T(1 - \eta T)/N\eta}$ compared to $\Delta_c T = \sqrt{T/N\eta}$ that is obtainable when using coherent states with an average photon number of N. Therefore, the photon number state is not just optimal in reducing the noise or uncertainty, but also useful against the photon loss in realistic transmission measurements. As the generation of Fock states with an arbitrary photon number N is not yet available with current technology, one can use instead N single photons relying on the equivalence to the case using an N photon number state in transmission measurement. Several studies have been carried out, such as absorption spectroscopy to analyze the organic dye molecule dibenzanthanthrene [38] or haemoglobin [39], and surface plasmon resonance sensing to measure the change

of the refractive index of an analyte under investigation with such Fock states [40].

In this work, we study theoretically and experimentally how much quantum enhancement can be obtained in measuring the optical activity of chiral molecular materials with single photons as an input state. We use a heralding scheme to generate the single-photon state that is linearly polarized and that illuminates sucrose solutions with different concentrations. To estimate the concentration of the sucrose solutions, we consider three typical polarimetric schemes: measurement of (i) the intensity of the horizontally polarized outgoing photons, (ii) the intensity difference between horizontally and vertically polarized outgoing photons, and (iii) the intensity difference-to-sum ratio (DSR) between the two linearly polarized outgoing photons. We analyse and compare the performances of these three schemes that use single-photon states to each other, but also to the optimal precision achievable with a classical input state. We find that type (iii) leads to the minimal estimation uncertainty compared to the other two types. A quantum enhancement, i.e. an improvement of the estimation precision when compared to measurement with a classical state of light is experimentally observed for both type (i) and type (ii) measurements. In general, our study proves that the quantum enhancement is always obtained at any η and T. The effect of experimental imperfections is also discussed, e.g. the extinction ratio of the optical components used in the experiment.

2. Experimental scheme

The experimental scheme used in this work is shown in figure 1(a). A continuous wave diode laser with a wavelength of 405 nm, filtered out at a later stage by a band pass filter and a long pass filter, pumps a non-linear crystal (a periodically poled potassium-titanyl-phosphate) to generate paired photons at the emission wavelengths of 809.6 nm and 810.4 nm with a full width at half maximum of 9.4 nm and 7.2 nm, respectively (see figure 1(b)). The two orthogonally polarized photons are spatially separated by a polarizing beam-splitter. One of the two photons, the vertically polarized idler photon, is directly sent to an avalanche photodiode single-photon detector (APD; SPCM-AQR-15, PerkinElmer). Quantum correlation between the photon pairs enables the click events from the idler detector APD_I to herald the horizontally polarized signal photon that is fed into the polarimetry set-up under investigation. Rotation of the linear polarization occurs when the signal photon passes through a sucrose solution. The magnitude of this rotation depends on the concentration of the sucrose solution, eventually determining the extent to which the polarization of the outgoing photons rotates. To make the scheme operate with heralded single photons in detection, we adopt a coincident measurement between APD_I and $APD_{H,V}$, i.e. the results of detection at $APD_{H,V}$ are recorded only when the single photons are detected at APD_I. Throughout this paper, let $N_{H,V}$ be the coincidence counts between APD_I and $APD_{H,V}$.

The heralded single-photon scheme is valid in the low gain parameter regime, where the state generated via spontaneous parametric down-conversion (SPDC) can be written
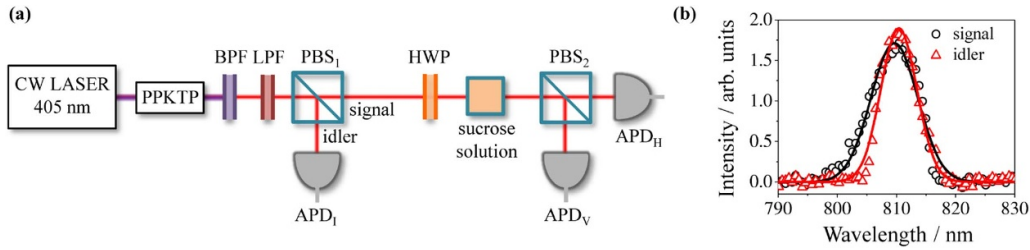
Figure 1. (a) Experimental scheme. A continuous-wave (CW) diode laser pumps a non-linear crystal (periodically poled potassium-titanyl-phosphate (PPKTP)) to produce photon pairs. The paired photons are orthogonally polarized and separated by the first polarizing beam-splitter (PBS₁). The pump beam is removed from the optical system using a band pass filter (BPF) and a long pass filter (LPF). The detection of a vertically (V) polarized photon at an avalanche photodiode in the idler channel (APD_I) heralds the generation of horizontally (H) polarized photons in the signal channel. The incident H-photons are rotated at a defined angle by a half-wave plate (HWP), and sent to a cuvette containing the sucrose solution under investigation. The polarization of the outgoing photons is analyzed via detection at APD_{H,V} placed in the output ports of the PBS₂. (b) The spectra of the photons generated by the SPDC process in the PPKTP. The central wavelengths of the signal and the idler photons are located at 809.6 nm and 810.4 nm, respectively.

as $|\text{SPDC}\rangle \approx |00\rangle + \epsilon|11\rangle$ with $|\epsilon| \ll 1$ [39]. The dead time of the APDs used in our experiment is ~60 ns and the time window of the field programmable gate array (FPGA), used for time-tracking analysis, is 25 ns. Considering these time-scales, we set the count rate of the idler photons to be about 8×10^5 cps by tuning the intensity of the pump laser. The sample size is set to $\nu = 10^5$, corresponding to the number of detection events in the idler port (APD_I), which heralds the twin photon in the signal port. We repeat the independent and identical measurement $\mu = 500$ times, assumed to be large enough to extract reliable statistical features of interest. Such sampling is applied to each polarization angle of incidence and each concentration of the sucrose solution.

The signal horizontal (H)-photons are rotated through a half wave plate, controlling the input polarization of θ_{in} in a range from $-100°$ to $100°$ in steps of $10°$. The input photons being linearly polarized at θ_{in} pass through sucrose solutions with concentrations C that vary from 0.1 g ml^{-1} to 0.6 g ml^{-1} in steps of 0.1 g ml^{-1}. The mirror asymmetry of the sucrose molecules induces a rotation of the linear polarization by α that depends in terms of its magnitude on the concentration C, resulting in outgoing photons with a linear polarization at $\theta_{\text{out}} = \theta_{\text{in}} + \alpha$. The latter is analyzed through decomposition into the H and vertical (V) polarizations, being realized by the polarizing beam-splitter. When either N_H or N_V only is measured, our scheme is equivalent to the conventional polarimetric scheme, where a linear polarizer is inserted and rotated before a detector while keeping the incident polarization the same.

The rotation angle α of the linear incident polarization as an effect of the optical activity is proportional to the solution concentration C and the propagation length l through the material, so the angle α can be written as

$$\alpha(\lambda) = [\alpha(\lambda)] \times l \times C, \qquad (1)$$

where $[\alpha(\lambda)]$ is the specific rotation of the sample material. The wavelength dependence in the specific rotation can be modelled by Drude's expression, written as

$$[\alpha(\lambda)] = \sum_j \frac{A_j}{\lambda^2 - \lambda_j^2}, \qquad (2)$$

where the summation is over multiple excitation transitions with λ_j and A_j being the resonance wavelength and the rotation amplitude for the jth transition, respectively. For the case of sucrose, the dispersion of the optical activity can be characterized by a single transition (i.e. $j = 1$), for which $A_1 = 2.1648 \times 10^7$ deg nm^2 dm^{-1} g^{-1} ml and $\lambda_1 = 146$ nm [22, 41]. We thus aim to estimate the concentration C from the measurement of the angle $\alpha(\lambda)$ for $l = 0.1$ dm (the length of the cuvette used in our experiment) and $[\alpha(\lambda)]$ given above.

In this work, we implement three kinds of estimators, yielding the associated f values, which are often used in classical polarimetry [9–11]: (i) the number N_H of the horizontally polarized photons transmitted through the sample, but normalized by ν; (ii) the difference $(N_H - N_V)$ between the horizontally and the vertically polarized photons transmitted through the sample, normalized by ν; and (iii) the difference $(N_H - N_V)$ normalized by the sum $(N_H + N_V)$, i.e. the DSR, which has recently been employed in imaging of non-uniform refractive profiles [42]. The expectation values of the above three estimators for ν single photons of incidence can be written, respectively, as

$$\text{(i)} \quad \langle f_{\text{single}} \rangle = \frac{\langle N_H \rangle}{\nu} = \eta_H \, T_{\theta_{\text{out}}}, \qquad (3)$$

$$\text{(ii)} \quad \langle f_{\text{diff}} \rangle = \frac{\langle N_H - N_V \rangle}{\nu} = \eta_H \, T_{\theta_{\text{out}}} - \eta_V \, R_{\theta_{\text{out}}}, \qquad (4)$$

$$\text{(iii)} \quad \langle f_{\text{DSR}} \rangle = \left\langle \frac{N_H - N_V}{N_H + N_V} \right\rangle \simeq \frac{\eta_H \, T_{\theta_{\text{out}}} - \eta_V \, R_{\theta_{\text{out}}}}{\eta_H \, T_{\theta_{\text{out}}} + \eta_V \, R_{\theta_{\text{out}}}}, \qquad (5)$$

where $\langle .. \rangle$ denotes an average with respect to the output state being measured and $\eta_{H,V}$ denote the efficiencies of transmission from the PPKTP to the detectors APD_{H,V} including the detection efficiencies. Here, $T_{\theta_{\text{out}}} = \cos^2\theta_{\text{out}}$ and $R_{\theta_{\text{out}}} = \sin^2\theta_{\text{out}}$ denote the transmittance and the reflectance for the outgoing single photon with a polarization of $\theta_{\text{out}} = \theta_{\text{in}} + \alpha$ to be transmitted through and reflected from the PBS₂ in figure 1, respectively. In particular, equation (5) asymptotically

holds for a large sample size ν, according to Jensen's inequality [43], which is the case in our experiment. In an ideal case where $\eta_H = \eta_V, N_H + N_V = \nu$, so that equation (5) becomes equation (4). The values $\eta_{H,V} \approx 0.25$ are explicitly measured by the coincidence count $N_{H,V}$ with scanning over θ_{in} when pure water is in the cuvette, i.e. $\alpha = 0$ (see the black curves and circles in figure 2), which exploits the correlated features of the SPDC photons as used in the Klyshko method [44–46].

In what follows, equations (3)–(5) are used to estimate the angle of rotation α from the measurement of the output polarization $\theta_{out} = \theta_{in} + \alpha$ for a given input polarization θ_{in}. The estimation of α subsequently leads to the estimation of the concentration C of sucrose solutions through equation (1). The impact of a finite concentration of the sucrose solution can be seen as a shift of the curve (for example, see the red curves and triangles in figure 2 for the measurement of the sucrose solution with a concentration of 0.5 g ml^{-1}). Assuming the values of $[\alpha]$, l, $\eta_{H,V}$, and θ_{in} to be accurately known beforehand, one can determine the estimation uncertainty ΔC directly by the estimation uncertainty of the output polarization $\Delta \theta_{out}$ extracted from the measurement of the outcome f.

3. Results and discussion

$\Delta \theta_{out}$ is experimentally obtained by the standard deviation of the estimated values θ_{out} from μ measurements with a sample size of ν, i.e. $\Delta \theta_{out}^{exp} = [\sum_j \theta_{out}^2/\mu - (\sum_j \theta_{out}/\mu)^2]^{1/2}$. The experimentally measured value $\Delta \theta_{out}^{exp}$ is compared to the theoretical prediction $\Delta \theta_{out}$, which can be calculated by considering the linear error propagation from the variance of the outcomes $\Delta f = \langle (\Delta f)^2 \rangle^{1/2}$ [47], written as

$$\Delta \theta_{out} = \frac{\Delta f}{\left| \frac{\partial \langle f \rangle}{\partial \theta_{out}} \right|}. \tag{6}$$

The variance $\langle (\Delta f)^2 \rangle$ can be calculated as

$$\langle (\Delta f)^2 \rangle = \sum_{j,k \in \{H,V\}} \frac{\partial \langle f \rangle}{\partial N_j} \frac{\partial \langle f \rangle}{\partial N_k} \mathrm{Cov}(N_j, N_k), \tag{7}$$

where $\mathrm{Cov}(N_j, N_k)$ is the covariance between the photon counts N_j and N_k. Equation (7) is an exact function for f_{single} and f_{diff}, but is an approximate function for f_{DSR} since equation (5) is a non-linear differential function of $N_{H,V}$ [48]. In our experiment, ν heralded single photons are used, and the theoretical expression of $\Delta \theta_{out}$ of equation (6) can be written, respectively, as

$$\Delta \theta_{out}^{single(q)} = \frac{1}{\sqrt{\nu}} \sqrt{\frac{1 - \eta_H T_{\theta_{out}}}{4\eta_H(1 - T_{\theta_{out}})}}, \tag{8}$$

$$\Delta \theta_{out}^{diff(q)} = \frac{1}{\sqrt{\nu}} \sqrt{\frac{(\eta_H T_{\theta_{out}} + \eta_V R_{\theta_{out}}) - (\eta_H T_{\theta_{out}} - \eta_V R_{\theta_{out}})^2}{4(\eta_H + \eta_V)^2 T_{\theta_{out}} R_{\theta_{out}}}}, \tag{9}$$
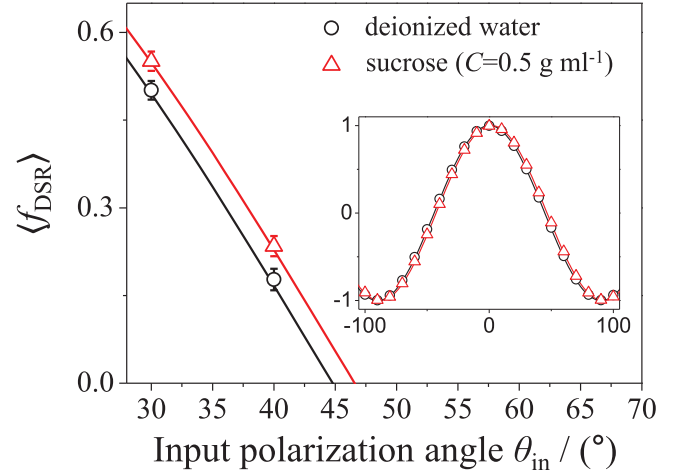
Figure 2. Open symbols show the measured $\langle f_{DSR} \rangle$ of equation (5) while varying the input polarization angle θ_{in} for deionized water (black circles) and for sucrose solution with $C = 0.5$ g ml^{-1} (red triangles). The inset shows the measured values in a full range of θ_{in} from $-100°$ to $100°$ in steps of $10°$. The horizontal displacement between the two sets of data exhibits the optical activity induced by the chiral material, enabling estimation of the rotation angle α. Solid curves are the fitted values using equation (10). The error bars are the standard deviation in the histogram over μ times of repetition at each value of θ_{in}.

$$\Delta \theta_{out}^{DSR(q)} = \frac{1}{\sqrt{\nu}} \sqrt{\frac{\eta_H T_{\theta_{out}} + \eta_V R_{\theta_{out}}}{4\eta_H \eta_V}}. \tag{10}$$
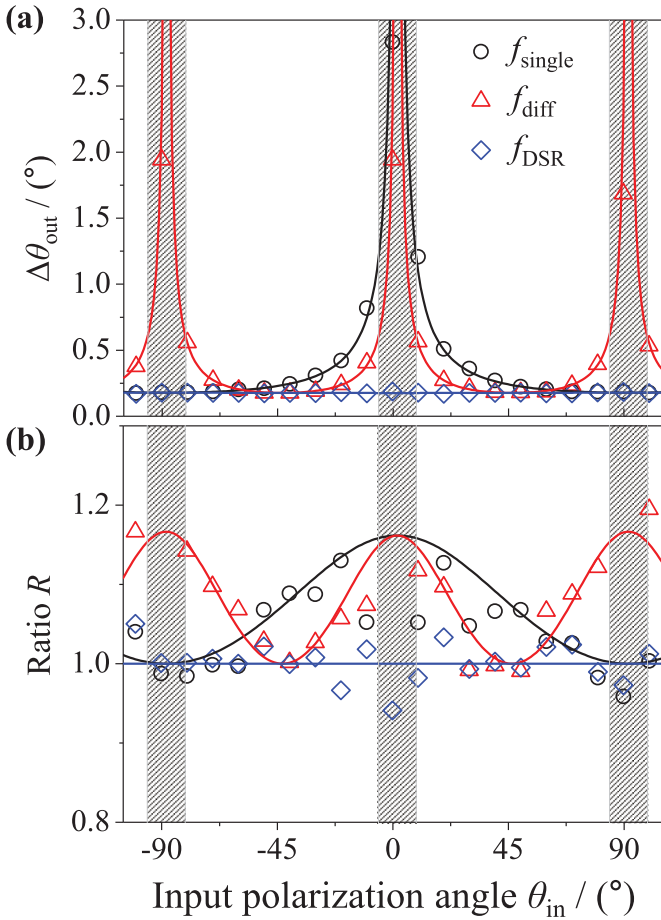
The uncertainties $\Delta \theta_{out}^{exp}$ are experimentally measured by using heralded single photons in the three schemes with varying θ_{in} for the sucrose solution with a concentration of 0.5 g ml^{-1} (see the open symbols in figure 3(a)). The experimentally measured uncertainties are compared with those calculated using equations (8)–(10) (see the solid curves in figure 3(a)), providing the analyses for the observed notable behaviors as a function of θ_{in}.

The two uncertainties $\Delta \theta_{out}^{single(q)}$ and $\Delta \theta_{out}^{diff(q)}$ diverge as $T_{\theta_{out}} \to 1$ (unless $\eta_H = 1$) and $T_{\theta_{out}} \to 0$ or 1 (unless $\eta_H = \eta_V = 1$), but decrease as $T_{\theta_{out}} \to 0$ and $T_{\theta_{out}} \to \eta_V(1 - \eta_V)/[\eta_V(1 - \eta_V) + \sqrt{\eta_H(1 - \eta_H)\eta_V(1 - \eta_V)}]$, respectively. At the latter limits, they have the minima: $\min[\Delta \theta_{out}^{single(q)}] = 1/(\sqrt{\nu}\sqrt{4\eta_H})$ and $\min[\Delta \theta_{out}^{diff(q)}] = [\eta_H(1 + \eta_V) + \eta_V(1 + \eta_H) + 2\sqrt{\eta_H(1 - \eta_H)\eta_V(1 - \eta_V)}]^{1/2}/(2\sqrt{\nu}(\eta_H + \eta_V))$. On the other hand, the uncertainty $\Delta \theta_{out}^{DSR(q)}$ has the minimum $\min[\Delta \theta_{out}^{DSR(q)}] = 1/(\sqrt{\nu}\sqrt{4\eta_H})$ at $T_{\theta_{out}} = 0$ and the maximum $\max[\Delta \theta_{out}^{DSR(q)}] = 1/(\sqrt{\nu}\sqrt{4\eta_V})$ at $T_{\theta_{out}} = 1$ when $\eta_H > \eta_V$. The minima and maxima are reversed when $\eta_V > \eta_H$. When $\eta_H = \eta_V \equiv \eta$, the uncertainty $\Delta \theta_{out}^{DSR(q)}$ takes a constant value $1/(\sqrt{\nu}\sqrt{4\eta})$ regardless of θ_{in}. Also note that

$$\min[\Delta \theta_{out}^{DSR(q)}] = \min[\Delta \theta_{out}^{single(q)}] < \min[\Delta \theta_{out}^{diff(q)}] \tag{11}$$

when $\eta_H > \eta_V$, whereas

$$\min[\Delta \theta_{out}^{DSR(q)}] < \min[\Delta \theta_{out}^{diff(q)}] < \min[\Delta \theta_{out}^{single(q)}] \tag{12}$$

Figure 3. (a) Experimentally measured estimation uncertainties (open symbols) of the output polarization angle $\Delta\theta_{\text{out}}$ with the three estimation schemes introduced in the main text, i.e. $\Delta\theta_{\text{out}}^{\text{DSR(q)}}$, $\Delta\theta_{\text{out}}^{\text{single(q)}}$, and $\Delta\theta_{\text{out}}^{\text{diff(q)}}$. They are in good agreement with the theoretical predictions (solid curves) using equations (8)–(10). The three schemes achieve almost the same minimal uncertainties since $\eta_{\text{H}} \approx \eta_{\text{V}}$ holds in our experiment, as expected from the theoretical analysis. (b) Relative quantum enhancement R with respect to the estimation uncertainties that would be obtained when probing the optical activity with a coherent state of light. Solid curves represent theoretical ratios R calculated by using equations (8)–(10) and equations (13)–(15). Importantly, the shaded regions are excluded, where the estimation is unphysical or malfunctioning due to a non-ideal extinction ratio of the polarizing beam splitter used in the experiment.

when $\eta_{\text{V}} > \eta_{\text{H}}$. For the equal efficiencies $\eta_{\text{V}} = \eta_{\text{H}}$, $\min[\Delta\theta_{\text{out}}^{\text{DSR(q)}}] = \min[\Delta\theta_{\text{out}}^{\text{single(q)}}] = \min[\Delta\theta_{\text{out}}^{\text{diff(q)}}]$. All this implies that the DSR scheme using equation (5) generally provides the optimal sensing scheme with the minimal uncertainty among the three estimators in any condition. The aforementioned theoretically expected behaviors are manifested in the experimentally measured values $\Delta\theta_{\text{out}}^{\text{exp}}$ and are shown in figure 3(a).

The classical benchmarks obtained with a coherent state with an average photon number of $\langle N \rangle = 1$ for the individual schemes are given by

$$\Delta\theta_{\text{out}}^{\text{single(c)}} = \frac{1}{\sqrt{\nu}}\sqrt{\frac{1}{4\eta_{\text{H}}(1 - T_{\theta_{\text{out}}})}}, \tag{13}$$

$$\Delta\theta_{\text{out}}^{\text{diff(c)}} = \frac{1}{\sqrt{\nu}}\sqrt{\frac{\eta_{\text{H}}T_{\theta_{\text{out}}} + \eta_{\text{V}}R_{\theta_{\text{out}}}}{4(\eta_{\text{H}} + \eta_{\text{V}})^2 T_{\theta_{\text{out}}}R_{\theta_{\text{out}}}}}, \tag{14}$$

$$\Delta\theta_{\text{out}}^{\text{DSR(c)}} = \frac{1}{\sqrt{\nu}}\sqrt{\frac{\eta_{\text{H}}T_{\theta_{\text{out}}} + \eta_{\text{V}}R_{\theta_{\text{out}}}}{4\eta_{\text{H}}\eta_{\text{V}}}}, \tag{15}$$

respectively. The relative quantum enhancement R can be quantified by the ratio of $\Delta\theta_{\text{out}}^{(\text{c})}$ to $\Delta\theta_{\text{out}}^{(\text{q})}$, written as

$$R = \frac{\Delta\theta_{\text{out}}^{(\text{c})}}{\Delta\theta_{\text{out}}^{(\text{q})}}. \tag{16}$$

Therefore, a value of R greater than unity exhibits a quantum enhancement. For the three schemes considered above, one can show that $R^{\text{single}} = (1 - \eta_{\text{H}}T_{\theta_{\text{out}}})^{-1/2}$, $R^{\text{diff}} = [1 - (\eta_{\text{H}}T_{\theta_{\text{out}}} - \eta_{\text{V}}R_{\theta_{\text{out}}})/(\eta_{\text{H}}T_{\theta_{\text{out}}} + \eta_{\text{V}}R_{\theta_{\text{out}}})]^{-1/2}$, and $R^{\text{DSR}} = 1$. Interestingly R is always equal to or greater than unity for all schemes considered in our experiment. These behaviors of the ratio R are presented in figure 3(b), given by the experimentally measured noise $\Delta\theta_{\text{out}}^{(q)}$ and the theoretical value $\Delta\theta_{\text{out}}^{(c)}$ that would be obtainable via the optimal classical polarimetry.

The estimators of equations (3)–(5) are unbiased under ideal conditions. One may wonder if the above estimation uncertainties evaluated using equation (6) reach the lower bound given by the Cramér–Rao (CR) inequality being satisfied for any unbiased estimator [49, 50]. The CR inequality can be written as $\Delta\theta_{\text{out}} \geq 1/\sqrt{\nu F(\theta_{\text{out}})}$ with $F(\theta_{\text{out}})$ being the Fisher information (FI) for a parameter θ_{out}. It depends on the measurement setting that is performed [51]. From the expressions of the FI (see appendix A) for both the classical and quantum schemes considered in this work, one can clearly see that the uncertainties evaluated using equation (6) are the same as the inverse of the squared FI regardless of $T_{\theta_{\text{out}}}$, $R_{\theta_{\text{out}}}$, and $\eta_{\text{H,V}}$ when estimating the parameter with the single-mode measurement scheme (i.e. f_{single}). However, the uncertainties of equation (6) with the two-mode measurement schemes (i.e. f_{diff} and f_{DSR}) are equal to or larger than the inverse of the squared FI. This implies that a better estimator than using f_{diff} and f_{DSR} exists when the photon-number-counting measurement is performed at the two modes.

When the measurement setting is optimized, the CR inequality can be further developed to be that called the quantum CR inequality, where the maximized FI is called the quantum FI (QFI) [47, 52]. For the output state decomposed into $\hat{\rho}_{\theta_{\text{out}}} = \sum_j p_j|\psi_j\rangle\langle\psi_j|$ with $\langle\psi_j|\psi_k\rangle = \delta_{j,k}$, it is known that the FI is the same as the QFI if $\partial_{\theta_{\text{out}}}|\psi_j\rangle = 0 \; \forall j$. Interestingly, the latter is the case for both the classical and quantum schemes considered in this work. This indicates that the photon-number-counting measurement is the optimal measurement scheme for both the classical and quantum approaches. This may not be true for other kinds of probe states, i.e. an individual optimal measurement scheme needs to be found and performed for maximization of quantum enhancement when other types of quantum states are illuminated into the sample.

Actual estimation of the concentration of sucrose solutions can be made via the relation $\theta_{\text{out}} = \langle\theta_{\text{in}}\rangle + \alpha$ and equation (1).
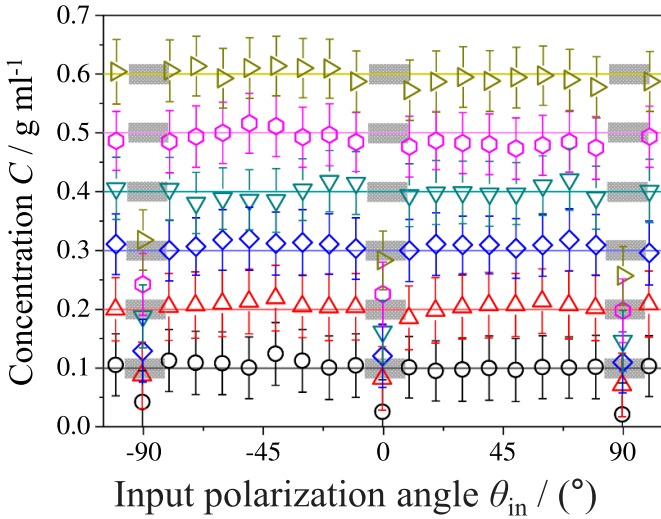
Figure 4. Experimentally estimated concentrations of sucrose solutions with six different concentrations are obtained by using the estimator of equation (5). We exclude the shaded regions as in figure 3, where the estimated concentrations are misleading due to a non-ideal extinction ratio (see appendix C for verification via a Monte-Carlo simulation). The error bar at individual points represents the standard deviation of the histogram obtained over μ times measurements.

Figure 4 shows the results of the scheme using the DSR estimator of equation (5) for sucrose solutions with different concentrations. The average estimated values C of the concentration are shown together with the estimation uncertainties ΔC. The latter reflects the type A uncertainties caused by probabilistic photon number counting. Further evaluation regarding uncertainties of other factors can be made, but we leave rigorous investigation of those minor contributions as a future work while providing the type B uncertainty budget in appendix B (see table B1). The shaded areas in figure 4 represent fallible regions which would lead to erroneous estimation, so we exclude those regions from the estimation.

It is worth discussing two experimental imperfections that led to the exclusion of the fallible regions in figures 3 and 4. First, the polarization control by experimental components may not be ideal, e.g. an incident H-photon to the polarizing beam splitter can exit through the V-photon output port. Its rate can be quantified by the polarization extinction (PE) ratio r_{PE}, which is measured to be about 1000/1 in our experiment. This means that even when $\theta_{out} = 0$, a few photons are found in APD$_V$ although no photon is supposed to be detected there in the ideal case. Such an imperfection becomes more significant as $T_{\theta_{out}} \to 0$ or 1, around which the estimation of the concentration C is likely to be more inaccurate. The effect of the PE is investigated via Monte-Carlo simulation (see the details in appendix C). We also identify that the imperfect functioning of experimental components can contribute to type A uncertainty. Second, particularly when the estimation is made with equation (3) at each incidence angle θ_{in}, the experimentally measured efficiency η_H is inserted into equation (3). This works reasonably well except for the cases when more than $\eta_H\nu$ photons are detected in the measurement

counting the photon number N_H. For example, consider the extreme yet possible case that all ν photons are detected in N_H even when $\eta_H < 1$. Note that photon loss occurs probabilistically with a probability η_H. In this case, $N_H/\eta_H\nu$ can be greater than unity and thus $T_{\theta_{out}} > 1$, leading to unphysical estimation. This arises because the value N_H/ν is divided by η_H, implying that the probabilistic nature associated with the efficiency η_H is regarded as a deterministic process that supposes only a definite number $\eta_H\nu$ of photons passes through an analyte, which is of course wrong and misses the probabilistic nature. Such an extreme case often take places when $T_{\theta_{out}} \to 1$ and similarly when $T_{\theta_{out}} \to 0$. The same concern also applies to the estimation with equation (4). Therefore, we exclude the range of θ_{out} such that $(\eta_{H,V}\nu - \langle N_{H,V}(\theta_{out})\rangle) < 3\langle\Delta N_{H,V}(\theta_{out})\rangle)$ for all the estimation schemes considered in this work in order to avoid inaccurate or unphysical estimation. The corresponding regimes are represented by shaded areas in figures 3 and 4.

The first issue could be alleviated by using optical components with as high a PE ratio r_{PE} as possible or at least a much better ratio on a logarithmic scale. The second issue, on the other hand, requires a more sophisticated modification to the estimation schemes. For example, one could perform simultaneous estimation of the concentration C and the efficiencies $\eta_{H,V}$ from the measurement with scanning through the incidence angles. This can typically be done by fitting equations (3)–(5) to the measured data, which we leave for future study.

4. Conclusion

We have experimentally investigated quantum polarimetric schemes using single-photon inputs to analyze the concentration of sucrose solutions. The horizontally and vertically polarized outgoing photons have been counted for each polarization of incidence and each concentration of sucrose solution in the experiment, leading to the determination of the optical activity. It has been shown that the minimal estimation uncertainty is generally achieved when the concentration is analyzed with a normalized difference between the horizontal and vertical photons, i.e. equation (5). We have discussed the quantum gain in the detection of the optical activity with respect to the three typical polarimetric schemes and the effects of the experimental and technical imperfections are identified.

When probing the optical activity with more intense light than a single-photon state and when it is, in addition, allowed and preferred for practical purposes, one may exploit bright squeezed states that can carry high optical powers [53]. In this case, the unit quantum enhancement per photon is still smaller when compared to single photons, but the overall quantum enhancement would be much higher due to the use of increased optical power (i.e. much larger N). Using bright squeezed states would provide practical quantum polarimetry in the high intensity regime, which we leave for future study. Quantum theory for the characterization of an arbitrary polarization in terms of Stokes parameters has recently been discussed and would be useful for further development of various quantum polarimetric schemes [54–56].

Acknowledgment

Appendix

Appendix A. Fisher information

Here we provide the calculation of the FI when the photon-number-counting measurement is performed at single-mode H or V, or at both modes, respectively. The FI can be written in terms of the probabilities of the measurement outcomes as

$$
F_{N_\mathrm{H}, N_\mathrm{V}}(\theta_\mathrm{out}) = \sum_{N_\mathrm{H}, N_\mathrm{V}} \frac{1}{p(N_\mathrm{H}, N_\mathrm{V}|\theta_\mathrm{out})} \left(\frac{\partial p(N_\mathrm{H}, N_\mathrm{V}|\theta_\mathrm{out})}{\partial \theta_\mathrm{out}} \right)^2
\tag{A1}
$$

when θ_out is estimated from measurement at the two modes. Similarly, when measurement is performed at either mode H or mode V, the FI can be written as

$$
F_{N_\mathrm{s}}(\theta_\mathrm{out}) = \sum_{N_\mathrm{s}} \frac{1}{p(N_\mathrm{s}|\theta_\mathrm{out})} \left(\frac{\partial p(N_\mathrm{s}|\theta_\mathrm{out})}{\partial \theta_\mathrm{out}} \right)^2,
\tag{A2}
$$

where $s \in \{\mathrm{H}, \mathrm{V}\}$. It can be easily shown that the associated probabilities are written as

$$
p^{(\mathrm{q})}(N_\mathrm{H}, N_\mathrm{V}) = \binom{N}{N_\mathrm{H}} \binom{N - N_\mathrm{H}}{N_\mathrm{V}} (\eta_\mathrm{H} T_{\theta_\mathrm{out}})^{N_\mathrm{H}} (\eta_\mathrm{V} R_{\theta_\mathrm{out}})^{N_\mathrm{V}}
$$
$$
\times (1 - \eta_\mathrm{H} T_{\theta_\mathrm{out}} - \eta_\mathrm{V} R_{\theta_\mathrm{out}})^{N - N_\mathrm{H} - N_\mathrm{V}},
\tag{A3}
$$

$$
p^{(\mathrm{q})}(N_\mathrm{H}) = \binom{N}{N_\mathrm{H}} (\eta_H T_{\theta_\mathrm{out}})^{N_\mathrm{H}} (1 - \eta_\mathrm{H} T_{\theta_\mathrm{out}})^{N - N_\mathrm{H}},
\tag{A4}
$$

$$
p^{(\mathrm{q})}(N_\mathrm{V}) = \binom{N}{N_\mathrm{V}} (\eta_\mathrm{V} R_{\theta_\mathrm{out}})^{N_\mathrm{V}} (1 - \eta_\mathrm{V} R_{\theta_\mathrm{out}})^{N - N_\mathrm{V}}
\tag{A5}
$$

for an N-photon number state of light, and

$$
p^{(\mathrm{c})}(N_\mathrm{H}, N_\mathrm{V})
$$
$$
= \mathrm{e}^{-\eta_\mathrm{H} T_{\theta_\mathrm{out}} N} \frac{(\eta_\mathrm{H} T_{\theta_\mathrm{out}} N)^{N_\mathrm{H}}}{N_\mathrm{H}!} \mathrm{e}^{-\eta_\mathrm{V} R_{\theta_\mathrm{out}} N} \frac{(\eta_\mathrm{V} R_{\theta_\mathrm{out}} N)^{N_\mathrm{V}}}{N_\mathrm{V}!},
\tag{A6}
$$

$$
p^{(\mathrm{c})}(N_\mathrm{H}) = \mathrm{e}^{-\eta_\mathrm{H} T_{\theta_\mathrm{out}} N} \frac{(\eta_\mathrm{H} T_{\theta_\mathrm{out}} N)^{N_\mathrm{H}}}{N_\mathrm{H}!},
\tag{A7}
$$

$$
p^{(\mathrm{c})}(N_\mathrm{V}) = \mathrm{e}^{-\eta_\mathrm{V} R_{\theta_\mathrm{out}} N} \frac{(\eta_\mathrm{V} R_{\theta_\mathrm{out}} N)^{N_\mathrm{V}}}{N_\mathrm{V}!}
\tag{A8}
$$

for a coherent state of light with an average photon number N. Substituting these probabilities into equations (A1) and (A2), one can write the FI for the quantum scheme as

$$
F_{N_\mathrm{H}, N_\mathrm{V}}^{(\mathrm{q})}(\theta_\mathrm{out}) = N \left(\frac{\eta_\mathrm{H}}{T_{\theta_\mathrm{out}}} + \frac{\eta_\mathrm{V}}{R_{\theta_\mathrm{out}}} \right) \left(\frac{\partial T_{\theta_\mathrm{out}}}{\partial \theta_\mathrm{out}} \right)^2
$$
$$
+ \frac{N(\eta_\mathrm{H} - \eta_\mathrm{V})^2}{1 - \eta_\mathrm{H} T_{\theta_\mathrm{out}} - \eta_\mathrm{V} R_{\theta_\mathrm{out}}} \left(\frac{\partial T_{\theta_\mathrm{out}}}{\partial \theta_\mathrm{out}} \right)^2, \tag{A9}
$$

$$
F_{N_\mathrm{H}}^{(\mathrm{q})}(\theta_\mathrm{out}) = \frac{N \eta_\mathrm{H}}{T_{\theta_\mathrm{out}} (1 - \eta_\mathrm{H} T_{\theta_\mathrm{out}})} \left(\frac{\partial T_{\theta_\mathrm{out}}}{\partial \theta_\mathrm{out}} \right)^2,
\tag{A10}
$$

$$
F_{N_\mathrm{V}}^{(\mathrm{q})}(\theta_\mathrm{out}) = \frac{N \eta_\mathrm{V}}{R_{\theta_\mathrm{out}} (1 - \eta_\mathrm{V} R_{\theta_\mathrm{out}})} \left(\frac{\partial T_{\theta_\mathrm{out}}}{\partial \theta_\mathrm{out}} \right)^2,
\tag{A11}
$$

and for the classical scheme as

$$
F_{N_\mathrm{H}, N_\mathrm{V}}^{(\mathrm{c})}(\theta_\mathrm{out}) = N \left(\frac{\eta_\mathrm{H}}{T_{\theta_\mathrm{out}}} + \frac{\eta_\mathrm{V}}{R_{\theta_\mathrm{out}}} \right) \left(\frac{\partial T_{\theta_\mathrm{out}}}{\partial \theta_\mathrm{out}} \right)^2,
\tag{A12}
$$

$$
F_{N_\mathrm{H}}^{(\mathrm{c})}(\theta_\mathrm{out}) = \frac{N \eta_\mathrm{H}}{T_{\theta_\mathrm{out}}} \left(\frac{\partial T_{\theta_\mathrm{out}}}{\partial \theta_\mathrm{out}} \right)^2,
\tag{A13}
$$

$$
F_{N_\mathrm{V}}^{(\mathrm{c})}(\theta_\mathrm{out}) = \frac{N \eta_\mathrm{V}}{R_{\theta_\mathrm{out}}} \left(\frac{\partial T_{\theta_\mathrm{out}}}{\partial \theta_\mathrm{out}} \right)^2,
\tag{A14}
$$

where $(\partial_{\theta_\mathrm{out}} T_{\theta_\mathrm{out}})^2 = 4 T_{\theta_\mathrm{out}} R_{\theta_\mathrm{out}}$ and $F(\theta_\mathrm{out}) = F(T_{\theta_\mathrm{out}}) \times (\partial_{\theta_\mathrm{out}} T_{\theta_\mathrm{out}})^2$ is used with $F(T_{\theta_\mathrm{out}})$ being the FI for the parameter T_{θ_out} for mathematical convenience. It is clear that the FI for the quantum scheme with a single-mode measurement is always greater than that for the classical scheme regardless of the values of T_{θ_out}, R_{θ_out}, and $\eta_{\mathrm{H,V}}$. The quantum scheme with two-mode measurement, on the other hand, is beneficial compared to the classical scheme only when $\eta_\mathrm{H} \neq \eta_\mathrm{V}$. Note again that the FI is the same as the QFI for both the classical and quantum schemes considered in this work, so the lower bounds to the uncertainty associated with equations (A9)–(A14) are ultimately optimal within the framework of the CR inequality.

Appendix B. Uncertainty budget

Here we provide the uncertainty budget for type A and B uncertainties [57], which have the potential to influence the estimation of concentration *C*. The relevant quantities in this work are the wavelength-dependent specific rotation, the length of the cuvette, and the angles such as θ_in and θ_out. For the specific rotation, we have used a fixed value of the wavelength in equation (2), but in reality no light is entirely monochromatic (i.e. see figure 1(b)), so that modulation of the wavelength in the reference calculation of the specific rotation needs to be considered in the estimation. Also, any realistic measurement of the length of the cuvette is far from ideal, so

Table B1. The uncertainty budgets of type A and B in our study. N and R represent the normal and rectangular distributions, respectively. This table is considered at $\theta_{\text{in}} = 40°$ and $C = 0.5$ g ml^{-1}.

Source of uncertainty	Value	Unit	Divisor (distribution)	Sensitivity	Standard uncertainty (g ml^{-1})
			(type A)		
θ_{out} obtained by f_{single}	0.2708	degree (°)	1 (N)	0.293	0.079 3
θ_{out} obtained by f_{diff}	0.1841	degree (°)	1 (N)	0.293	0.053 9
θ_{out} obtained by f_{DSR}	0.1763	degree (°)	1 (N)	0.293	0.051 7
			(type B)		
Specific rotation $[\alpha(\lambda)]$	0.41	°dm^{-1}g^{-1}ml	1 (N)	0.05	0.0205
Length of cuvette l	0.0005	dm	1.732 (R)	17.07	0.004 9
Input polarization θ_{in}	0.03	degree (°)	1 (N)	0.586	0.017 6
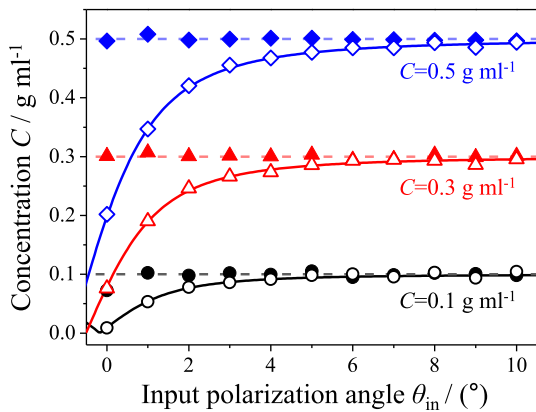
Figure C1. The results of the Monte-Carlo simulation to estimate the concentration C using equation (5) for two cases: $r_{\text{PE}} = 1000/1$ (open symbols) and $r_{\text{PE}} \rightarrow \infty$ (closed symbols). Solid lines represents the analytical values obtained using equations (C3), (C6), and (C7), whereas the dashed lines are the true values of the concentration ($C = 0.1, 0.3,$ and 0.5 g ml^{-1}) used in the simulation. Here, $\eta_{\text{H,V}} = 0.25$, $\nu = 10^5$, and $\mu = 500$ are used.

the length might be slightly different from the assumed value of 0.1 dm. A similar behavior would be observed in the calibration of θ_{in}. These effects are treated as type B uncertainty, whereas the measurement of θ_{out} is actually repeated, leading to type A uncertainty evaluation. Such relevant uncertainties are listed in table B1 for further information.

Appendix C. Monte-Carlo simulation

To understand the effects of the experimental imperfections involved in the results shown in figures 3 and 4, we perform a Monte-Carlo simulation by varying the relevant parameters, in an arbitrary range, which are typically constrained in a real experiment. The concentration is estimated from the data obtained through the numerical simulation by varying the input polarization θ_{in} from 0° to 10° in steps of 1°, providing a detailed study in the shaded area in figures 3 and 4. In order to see the effect of the PE in the estimation, we compare the case of an ideal extinction ratio ($r_{\text{PE}} \rightarrow \infty$) with the case of a realistic extinction ratio ($r_{\text{PE}} = 1000/1$) for $C = 0.1, 0.3,$ and 0.5 g ml^{-1}, shown in figure C1. It is shown that the estimated concentration is equal to the true value up to the numerical

precision of sampling in the ideal case, whereas it drops down at $\theta_{\text{out}} = \theta_{\text{in}} + \alpha \approx 0°$—the effect of PE is maximal, indicating an erroneous estimation in the realistic case. The effect of PE becomes less significant as $T_{\theta_{\text{out}}}$ approaches 1/2 since the PE of H- and V-photons takes place almost symmetrically and thus compensates each other. Furthermore, note that a little deviation from the true value occurs at $\theta_{\text{out}} \approx 0°$ even in the ideal case. Such an error can be shown to be independent of ν and μ, and rather is a technical problem related to using the inverse function of equation (5) to estimate θ_{out}. It has been overwhelmed by the effect of PE ($r_{\text{PE}} \sim 1000/1$) in the measured data shown in figures 3 and 4.

The observed behaviors shown in figure C1 can be explained via an appropriate modification to the theoretical development made in the main text. The effect of PE, i.e. the erroneous exchange between the H-photon and the V-photon with a rate r_{PE}, can be included in the theory by replacing $T_{\theta_{\text{out}}}$ by $T_{\theta_{\text{out}}} + r_{\text{PE}} \times \delta T_{\theta_{\text{out}}}$, where $\delta T_{\theta_{\text{out}}} = 1 - 2T_{\theta_{\text{out}}}$. Equations (3)–(5) can thus be written up to the first order of $r_{\text{PE}} \ll 1$ as

$$\text{(i)} \qquad \frac{\langle N_{\text{H}} \rangle}{\nu} \approx \langle f_{\text{single}} \rangle + r_{\text{PE}} \times \delta f_{\text{single}}, \qquad \text{(C1)}$$

$$\text{(ii)} \qquad \frac{\langle N_{\text{H}} - N_{\text{V}} \rangle}{\nu} \approx \langle f_{\text{diff}} \rangle + r_{\text{PE}} \times \delta f_{\text{diff}}, \qquad \text{(C2)}$$

$$\text{(iii)} \qquad \left\langle \frac{N_{\text{H}} - N_{\text{V}}}{N_{\text{H}} + N_{\text{V}}} \right\rangle \approx \langle f_{\text{DSR}} \rangle + r_{\text{PE}} \times \delta f_{\text{DSR}}, \qquad \text{(C3)}$$

where

$$\delta f_{\text{single}} = (1 - 2T_{\theta_{\text{out}}})\eta_{\text{H}}, \qquad \text{(C4)}$$

$$\delta f_{\text{diff}} = (1 - 2T_{\theta_{\text{out}}})(\eta_{\text{H}} + \eta_{\text{V}}), \qquad \text{(C5)}$$

$$\delta f_{\text{DSR}} = (1 - 2T_{\theta_{\text{out}}}) \frac{2\eta_{\text{H}}\eta_{\text{V}}}{[T_{\theta_{\text{out}}}\eta_{\text{H}} + (1 - T_{\theta_{\text{out}}})\eta_{\text{V}}]^2}. \qquad \text{(C6)}$$

It is clear to see that the effect of the PE for the three estimators is maximal when $T_{\theta_{\text{out}}} = 0$ or 1, whereas it vanishes when $T_{\theta_{\text{out}}} = 1/2$.

All the errors δf in equations (C4)–(C6) lead to an equal amount of error in the estimation of θ_{out}, i.e. $\theta_{\text{out}} \to \theta_{\text{out}} + r_{\text{PE}} \delta \theta_{\text{out}}$, where the error

$$\delta \theta_{\text{out}} = \frac{\cos 2\theta_{\text{out}}}{|\sin 2\theta_{\text{out}}|} = \frac{2T_{\theta_{\text{out}}} - 1}{2\sqrt{T_{\theta_{\text{out}}}(1 - T_{\theta_{\text{out}}})}}. \qquad (C7)$$

The error $\delta \theta_{\text{out}}$ caused by the PE diverges as $T_{\theta_{\text{out}}} \to 0$ or 1, while it decreases as $T_{\theta_{\text{out}}}$ approaches 1/2.

The PE consequently causes an error in the uncertainty $\Delta \theta_{\text{out}}$ of equations (8)–(10), i.e. $\Delta \theta_{\text{out}} \to \Delta \theta_{\text{out}} + r_{\text{PE}} \times \delta \Delta \theta_{\text{out}}$, where $\delta \Delta \theta_{\text{out}}$ can be found as

$$\delta \Delta \theta_{\text{out}}^{\text{single(q)}} = \frac{1}{\sqrt{\nu}} \frac{1 - 2T_{\theta_{\text{out}}}}{8} \left(\frac{1}{\eta_{\text{H}}} - 1 \right) \frac{1}{(1 - T_{\theta_{\text{out}}})^2} \frac{1}{\Delta \theta_{\text{out}}^{\text{single(q)}}}, \quad (C8)$$

$$\delta \Delta \theta_{\text{out}}^{\text{diff(q)}} = \frac{1}{\sqrt{\nu}} \frac{1 - 2T_{\theta_{\text{out}}}}{8} \frac{1}{(\eta_{\text{H}} + \eta_{\text{V}})^2}$$
$$\times \left(\frac{\eta_{\text{H}}(1 - \eta_{\text{H}})}{(1 - T_{\theta_{\text{out}}})^2} - \frac{\eta_{\text{V}}(1 - \eta_{\text{V}})}{T_{\theta_{\text{out}}}^2} \right) \frac{1}{\Delta \theta_{\text{out}}^{\text{diff(q)}}}, \quad (C9)$$

$$\delta \Delta \theta_{\text{out}}^{\text{DSR(q)}} = \frac{1}{\sqrt{\nu}} \frac{1 - 2T_{\theta_{\text{out}}}}{8} \left(\frac{1}{\eta_{\text{V}}} - \frac{1}{\eta_{\text{H}}} \right) \frac{1}{\Delta \theta_{\text{out}}^{\text{DSR(q)}}}. \quad (C10)$$

ORCID iDs

Changhyoup Lee ⬤ https://orcid.org/0000-0002-1401-4230
Kwang-Geol Lee ⬤ https://orcid.org/0000-0002-9795-4403

References

[1] Hutt A J and Tan S C 1996 Drug chirality and its clinical significance *Drugs* **52** 1
[2] Zhao Y, Askarpour A N, Sun L, Shi J, Li X and Alù A 2017 Chirality detection of enantiomers using twisted optical metamaterials *Nat. Commun.* **8** 14180
[3] Lough W J and Wainer I W 2002 Chirality in Natural and Applied Science (Oxford: Blackwell Science)
[4] Amabilino D B 2009 *Chirality at the Nanoscale: Nanoparticles, Surfaces, Materials and More* (Weinheim: Wiley-VCH)
[5] Barron L D 2009 *Molecular Light Scattering and Optical Activity* (Cambridge: Cambridge University Press)
[6] Schäferling M 2017 *Chiral Nanophotonics* (Berlin: Springer)
[7] Hentschel M, Schäferling M, Duan X, Giessen H and Liu N 2017 Chiral plasmonics *Sci. Adv.* **3** e1602735
[8] Fernandez-Corbaton I, Rockstuhl C, Ziemke P, Gumbsch P, Albiez A, Schwaiger R, Frenzel T, Kadic M and Wegener M 2019 New twists of 3D chiral metamaterials *Adv. Mater.* **31** 1807742
[9] Carroll B and Blei I 1963 Measurement of optical activity: new approaches *Science* **142** 200
[10] Chou C, Tsai H-M, Liao K-Y, Chou L-D and Huang P-H 2006 Optical activity measurement by use of a balanced detector optical heterodyne interferometer *Appl. Opt.* **45** 3733
[11] Castiglioni E, Abbate S and Longhi G 2011 Experimental methods for measuring optical rotatory dispersion: survey and outlook *Chirality* **23** 711
[12] Neuman K C, Chadd E H, Liou G F, Bergman K and Block S M 1999 Characterization of photodamage to *Escherichia coli* in optical traps *Biophys. J.* **77** 2856
[13] Peterman E J G, Gittes F and Schmidt C F 2003 Laser-induced heating in optical traps *Biophys. J.* **84** 1308
[14] Taylor M 2015 *Quantum Microscopy of Biological Systems* (Berlin: Springer)
[15] Taylor M A and Bowen W P 2016 Quantum metrology and its application in biology *Phys. Rep.* **615** 1
[16] Wolfgramm F, Cerè A, Beduini F A, Predojević A, Koschorreck M and Mitchell M W 2010 Squeezed-light optical magnetometry *Phys. Rev. Lett.* **105** 053601
[17] Roccia E, Cimini V, Sbroscia M, Gianani I, Ruggiero L, Mancino L, Genoni M G, Ricci M A and Barbieri M 2018 Multiparameter approach to quantum phase estimation with limited visibility *Optica* **5** 1171
[18] Giovannetti V, Lloyd S and Maccone L 2004 Quantum-enhanced measurements: beating the standard quantum limit *Science* **306** 1330
[19] Paris M G A 2009 Quantum estimation for quantum technology *Int. J. Quantum Inf.* **7** 125
[20] Giovannetti V, Lloyd S and Maccone L 2011 Advances in quantum metrology *Nat. Photonics* **5** 222
[21] Wolfgramm F, Vitelli C, Beduini F A, Godbout N and Mitchell M W 2013 Entanglement-enhanced probing of a delicate material system *Nat. Photonics* **7** 28
[22] Tischler N, Krenn M, Fickler R, Vidal X, Zeilinger A and Molina-Terriza G 2016 Quantum optical rotatory dispersion *Sci. Adv.* **2** e1601306
[23] Cimini V *et al* 2019 Quantum sensing for dynamical tracking of chemical processes *Phys. Rev.* A **99** 053817
[24] Cimini V, Mellini M, Rampioni G, Sbroscia M, Leoni L, Barbieri M and Gianani I 2019 Adaptive tracking of enzymatic reactions with quantum light *Opt. Express* **27** 35245
[25] Crespi A, Lobino M, Matthews J C F, Politi A, Neal C R, Ramponi R, Osellame R and O'Brien J L 2012 Measuring protein concentration with entangled photons *Appl. Phys. Lett.* **100** 233704
[26] D'Angelo M, Chekhova M V and Shih Y 2001 Two-photon diffraction and quantum lithography *Phys. Rev. Lett.* **87** 013602
[27] Ono T, Okamoto R and Takeuchi S 2013 An entanglement-enhanced microscope *Nat. Commun.* **4** 2426
[28] Israel Y, Rosen S and Silberberg Y 2014 Supersensitive polarization microscopy using N00N states of light *Phys. Rev. Lett.* **112** 103604
[29] Dowling J P 2008 Quantum optical metrology—the lowdown on high-N00N states *Contemp. Phys.* **49** 125
[30] Chen Y *et al* 2018 Quantum plasmonic N00N state in a silver nanowire and its use for quantum sensing *Optica* **5** 1229
[31] Dorner U, Demkowicz-Dobrzanski R, Smith B J, Lundeen J S, Wasilewski W, Banaszek K and Walmsley I A 2009 Optimal quantum phase estimation *Phys. Rev. Lett.* **102** 040403
[32] Kacprowicz M, Demkowicz-Dobrzański R, Wasilewski W, Banaszek K and Walmsley I A 2010 Experimental quantum-enhanced estimation of a lossy phase shift *Nat. Photonics* **4** 357
[33] Lee C, Dieleman F, Lee J, Rockstuhl C, Maier S A and Tame M 2016 Quantum plasmonic sensing: beyond the shot-noise and diffraction limit *ACS Photonics* **3** 992

[34] Monras A and Paris M G A 2007 Optimal quantum estimation of loss in bosonic channels *Phys. Rev. Lett.* **98** 160401

[35] Alipour S, Mehboudi M and Rezakhani A T 2014 Quantum metrology in open systems: dissipative Cramér–Rao bound *Phys. Rev. Lett.* **112** 120405

[36] Meda A, Losero E, Samantaray N, Scafirimuto F, Pradyumna S, Avella A, Ruo-Berchera I and Genovese M 2017 Photon-number correlation for quantum enhanced imaging and sensing *J. Opt.* **19** 094002

[37] Adesso G, Dell'Anno F, De Siena S, Illuminati F and Souza L A M 2009 Optimal estimation of losses at the ultimate quantum limit with non-Gaussian states *Phys. Rev.* A **79** 040305

[38] Rezus Y L A, Walt S G, Lettow R, Renn A, Zumofen G, Götzinger S and Sandoghdar V 2012 Single-photon spectroscopy of a single molecule *Phys. Rev. Lett.* **108** 093601

[39] Whittaker R, Erven C, Neville A, Berry M, O'Brien J L, Cable H and Matthews J C F 2017 Absorption spectroscopy at the ultimate quantum limit from single-photon states *New J. Phys.* **19** 023013

[40] Lee J-S, Yoon S-J, Rah H, Tame M, Rockstuhl C, Song S H, Lee C and Lee K-G 2018 Quantum plasmonic sensing using single photons *Opt. Express* **26** 29272

[41] Lowry T M and Richards E M 1924 CCCXLVI—the rotatory dispersive power of organic compounds. Part XIII. The significance of simple rotatory dispersion. Rotatory dispersion of camphorquinone and of sucrose *J. Chem. Soc. Trans.* **125** 2511

[42] Ortolano G, Ruo-Berchera I and Predazzi E 2020 Quantum enhanced imaging of nonuniform refractive profiles *Int. J. Quantum Inf.* **17** 1941010

[43] Jensen J L W V 1906 Surles fonctions convexes et les inégalités entre les valeurs moyennes *Acta Math.* **30** 175

[44] Klyshko D N 1980 Use of two-photon light for absolute calibration of photoelectric detectors *Sov. J. Quantum Electron.* **10** 1112

[45] Burnham D C and Weinberg D L 1970 Observation of simultaneity in parametric production of optical photon pairs *Phys. Rev. Lett.* **25** 84

[46] Rarity J G, Ridley K D and Tapster P R 1987 Absolute measurement of detector quantum efficiency using parametric downconversion *Appl. Opt.* **26** 4616

[47] Braunstein S L and Caves C M 1994 Statistical distance and the geometry of quantum states *Phys. Rev. Lett.* **72** 3439

[48] Abayzeed S A, Smith R J, See C W and Somekh M G 2018 Analysis of noise in differential and ratiometric biosensing systems *Sens. Actuators* B **260** 1059

[49] Durkin G A and Dowling J P 2007 Local and global distinguishability in quantum interferometry *Phys. Rev. Lett.* **99** 070801

[50] Pezzè L, Smerzi A, Oberthaler M K, Schmied R and Treutlein P 2018 Quantum metrology with nonclassical states of atomic ensembles *Rev. Mod. Phys.* **90** 035005

[51] Cramér H 1999 *Mathematical Methods of Statistics* (Princeton, NJ: Princeton University Press)

[52] Braunstein S L, Caves C M and Milburn G J 1996 Generalized uncertainty relations: theory, examples and Lorentz invariance *Ann. Phys. (NY)* **247** 135

[53] Lawrie B J, Lett P D, Marino A M and Pooser R C 2019 Quantum sensing with squeezed light *ACS Photonics* **6** 1307

[54] Ling A, Soh K P, Lamas-Linares A and Kurtsiefer C 2006 An optimal photon counting polarimeter *J. Mod. Opt.* **53** 1523

[55] Goldberg A Z and James D F V 2018 Quantum-limited Euler angle measurements using anticoherent states *Phys. Rev.* A **98** 032113

[56] Goldberg A. Z. 2020 Quantum theory of polarimetry: From quantum operations to Mueller matrices. *Phys. Rev. Research* **2** 023038

[57] BIPM, IEC, IFCC, ILAC, ISO, IUPAC, IUPAP and OIML 2008 *Evaluation of measurement data Guide to the Expression of Uncertainty in Measurement* (Joint Committee for Guides in Metrology vol 100) (Geneve: International Organization for Standardization)